Title: Impaired immune signaling and changes in the lung microbiome precede secondary bacterial pneumonia in COVID-19

Authors:

†Alexandra Tsitsiklis[1], †Beth Shoshana Zha[2], †Ashley Byrne[3], †Catherine DeVoe[1], †Elze Rackaityte[4], Sophia Levan[5], Sara Sunshine[5], Eran Mick[1,2,3], Rajani Ghale[1,2], Christina Love[1,2], Alexander J. Tarashansky[3], Angela Pisco[3], Jack Albright[3], Alejandra Jauregui[2], Aartik Sarma[2], Norma Neff[3], Paula Hayakawa Serpa[1], Thomas J. Deiss[2], Amy Kistler[3], Sidney Carrillo[2], K. Mark Ansel[6,7], Aleksandra Leligdowicz[2], Stephanie Christenson[2], Angela Detweiler[3], Norman G. Jones[8], Bing Wu[9], Spyros Darmanis[9], Susan V. Lynch[10,11], Joseph L. DeRisi[3,4], COMET Consortium+, Michael A. Matthay[2], Carolyn M. Hendrickson[2], Kirsten N. Kangelaris[5], Matthew F. Krummel[12], Prescott G. Woodruff[2,7], David J. Erle[5,13,14], Oren Rosenberg[1], Carolyn S. Calfee[2], *Charles R. Langelier[1,3]

†equal contributions

Affiliations:

[1] Department of Medicine, Division of Infectious Diseases, University of California San Francisco, San Francisco, CA, USA

[2] Department of Medicine, Division of Pulmonary, Critical Care, Allergy and Sleep Medicine, University of California San Francisco, San Francisco, CA, USA

[3] Chan Zuckerberg Biohub, San Francisco, CA, USA

[4] Department of Biochemistry and Biophysics, University of California San Francisco, San Francisco, CA, USA

[5] Department of Medicine, University of California San Francisco, San Francisco, CA, USA

[6] Department of Microbiology and Immunology, University of California, San Francisco, CA, USA

27 [7] Sandler Asthma Basic Research Center, University of California, San Francisco, CA, USA

28 [8] Department of Experimental Medicine, University of California, San Francisco, CA, USA

29 [9] Genentech, Inc. San Francisco, CA, USA.

30 [10] Department of Gastroenterology, University of California, San Francisco, CA, USA

31 [11] Benioff Center for Microbiome Medicine, University of California, San Francisco, CA, USA

32 [12] Department of Pathology, University of California, San Francisco, CA, USA

33 [13] Lung Biology Center, University of California, San Francisco, CA, USA

34 [14] UCSF CoLabs, University of California, San Francisco, CA, USA

35 [+]COMET (COVID-19 Multiphenotyping for Effective Therapies) Consortium members are listed

36 in the Supplementary Appendix.

37

38

39 *Corresponding author: Charles R. Langelier

40 Address: 499 Illinois Street, San Francisco, CA 94058

41 Phone: 801-201-5049

42 Email: chaz.langelier@ucsf.edu

43

44

45 Conflict of interest: The authors have declared that no conflict of interest exists.

46

Abstract

Secondary bacterial infections, including ventilator-associated pneumonia (VAP), lead to worse clinical outcomes and increased mortality following viral respiratory infections including in patients with coronavirus disease 2019 (COVID-19). Using a combination of tracheal aspirate bulk and single-cell RNA sequencing we assessed lower respiratory tract immune responses and microbiome dynamics in 23 COVID-19 patients, 10 of whom developed VAP, and eight critically ill uninfected controls. At a median of three days (range: 2-4 days) before VAP onset we observed a transcriptional signature of bacterial infection. At a median of 15 days prior to VAP onset (range: 8-38 days), we observed a striking impairment in immune signaling in COVID-19 patients who developed VAP. Longitudinal metatranscriptomic analysis revealed disruption of lung microbiome community composition in patients with VAP, providing a connection between dysregulated immune signaling and outgrowth of opportunistic pathogens. These findings suggest that COVID-19 patients who develop VAP have impaired antibacterial immune defense detectable weeks before secondary infection onset.

61 **Introduction**

62 Secondary bacterial pneumonia results in significant morbidity and mortality in patients
63 with viral lower respiratory tract infections (LRTI)[1]. This problem was evident in the 1918 influenza
64 pandemic during which the majority of deaths were ultimately attributed to secondary bacterial
65 pneumonia[2]. SARS-CoV-2 infection, like influenza, confers an increased risk of late onset
66 secondary bacterial infection, often manifesting as ventilator-associated pneumonia (VAP)[3,4].
67 Marked heterogeneity exists, however, with respect to the risk of VAP in patients with coronavirus
68 disease 2019 (COVID-19), with incidence ranging from 12-87% in published cohort studies[5–8].

69 The mechanisms underlying VAP susceptibility in COVID-19 remain unknown. Animal
70 models of influenza may provide some insight, suggesting a role for interferon-mediated
71 suppression of cytokines essential for bacterial defense, including those important for neutrophil
72 recruitment, antimicrobial peptide production and the Th17 response[9–11]. The impact of interferon
73 signaling on antibacterial host defense, however, varies based on bacterial pathogen, and is not
74 well studied in humans[12].

75 Much of our understanding of VAP immunobiology derives from sepsis studies, which
76 describe a state of immune reprogramming in patients who go on to develop nosocomial
77 infections[13–16]. This state is characterized by impaired monocyte, neutrophil and CD4 lymphocyte
78 function, as well as decreased responsiveness of pathogen recognition receptors and
79 downstream signaling pathways[13–16]. Severe COVID-19, like sepsis, is characterized by a
80 dysregulated host response to infection, raising the possibility that similar mechanisms may
81 contribute to the development of VAP in patients infected with SARS-CoV-2.

82 In addition to host immune elements, microbial factors contribute to VAP pathogenesis.
83 Mechanically ventilated patients endure prolonged exposure to the hospital environment, which
84 increases risk of colonization by opportunistic pathogens in the upper airway, oropharynx, and
85 lungs[14,16]. Micro-aspiration or direct invasion may subsequently lead to lower respiratory tract
86 disease and clinical onset of VAP[16,17]. Further, the common practice of early empiric antimicrobial

87 administration in critically ill patients can lead to disruption of the lung microbiome, which has
88 been associated with the development of VAP[18,19].

89 Despite their interconnected roles, no studies to date have simultaneously profiled host
90 immune responses and lung microbiome dynamics in the context of VAP. Further, the question
91 of whether host responses to SARS-CoV-2 or other viral infections may contribute to this
92 dysbiosis, leading to VAP, remains unanswered.

93 Given the marked heterogeneity in VAP incidence among patients with COVID-19[5–8], as
94 well as gaps in mechanistic understanding of secondary bacterial pneumonia, we sought to
95 assess the molecular determinants of VAP in patients infected with SARS-CoV-2. We employed
96 a systems biology approach involving immunoprofiling the host transcriptional response and
97 simultaneously assessing lung microbiome dynamics, using a combination of bulk and single cell
98 RNA sequencing and extensive clinical phenotyping. We observed a striking impairment in
99 antibacterial immune signaling at the time of intubation, that correlated with disruption of the lung
100 microbiome, weeks before the onset of VAP.

101

102 **Results**

103 We conducted a prospective case-control study of adults requiring mechanical ventilation
104 for COVID-19 or for illnesses other than pneumonia. Of 63 patients with COVID-19 initially
105 enrolled, tracheal aspirate (TA) specimens from 23 patients met inclusion criteria for primary
106 analysis (**Methods, Figure 1)**. In addition, eight critically ill patients without COVID-19 from a
107 second cohort (Study 2, **Methods**) were included as controls. Patients were enrolled at one
108 tertiary care hospital and one safety net hospital in San Francisco, California under research
109 protocols approved by the University of California San Francisco Institutional Review Board
110 **(Methods)**. We collected TA periodically following intubation and performed bulk and single cell
111 RNA-seq (scRNA-seq) **(Methods)**.

112 Patients with VAP were adjudicated using the United States Centers for Disease Control
113 (CDC) definition[20], including a requirement for a positive bacterial TA culture (n=10). We defined
114 onset of VAP as the first day a patient developed any of the criteria used to meet the definition,
115 in accordance with CDC guidance[20]. Patients who did not meet the CDC criteria for VAP, and for
116 whom there was no sustained clinical suspicion for bacterial pneumonia during the admission,
117 were adjudicated as No-VAP (n=13). Patients who met CDC VAP criteria but had negative
118 bacterial TA cultures, patients who were clinically suspected of having VAP with either positive or
119 negative TA cultures, and patients who met clinical pneumonia criteria on intubation were
120 excluded from this study **(Figure 1)**.

121 We compared lower respiratory tract host transcriptional responses between the VAP and
122 No-VAP groups at two timepoints. “Early” timepoint TA samples were collected a median of two
123 days post-intubation and 17 days before VAP onset (range: 15-38 days) for bulk RNA-seq
124 analyses or 10 days before VAP onset (range: 8-16 days) for scRNA-seq analyses. “Late”
125 timepoint samples were collected a median of two days before VAP onset (range: 2-3 days) for
126 bulk RNA-seq analyses and three days before VAP onset (range: 2-4 days) for scRNA-seq
127 analyses, and compared against samples collected from No-VAP patients at similar timepoints
128 post-intubation (**Figure 1, Table 1**). No samples were analyzed after the onset of VAP. We
129 additionally evaluated eight intubated patients with non-pneumonia illnesses as controls at the
130 “early” timepoint.

131 We considered that sex as a biologic variable is important for acute COVID-19 severity,
132 and thus asked whether differences in sex might explain our observations. However, no
133 differences in sex were present between VAP and No-VAP groups (P=1, early and late timepoints)
134 **(Table 1)**. There were also no significant differences between groups with respect to age, race or
135 ethnicity **(Table 1, S1, S2)**. In addition, there were no differences between groups with respect to
136 in-hospital receipt of any immunosuppressant or antibiotics prior to sample collection (**Table S1,**
137 **S2, S3**).

138 **COVID-19 VAP is associated with a transcriptional signature of bacterial infection two days**
139 **before VAP onset**

140 We began by assessing the lower respiratory host transcriptional response at the "late"
141 timepoint, just before VAP onset. We carried out differential gene expression analysis on TA bulk
142 RNA-seq data from five patients who developed VAP and eight No-VAP patients **(Table 1)**. We
143 identified 436 differentially expressed genes at a False Discovery Rate (FDR) < 0.1 **(Figure 2A)**
144 and performed gene set enrichment analysis (GSEA) **(Figure 2B)**.

145 As expected, the VAP group exhibited upregulation of pathways related to antibacterial
146 immune responses in the days preceding secondary infection, such as neutrophil degranulation,
147 toll-like receptor signaling, cytokine signaling and antigen presentation **(Figure 2B)**. We also
148 noted that interferon alpha/beta signaling was upregulated. Ingenuity pathway analysis (IPA)
149 predicted broad activation of upstream inflammatory cytokines (including IFNα and IFNγ) in the
150 VAP group at this "late" timepoint **(Figure 2C)**.

151

152 **COVID-19 patients who develop VAP have attenuated immune signaling two weeks before**
153 **VAP onset**

154 Given our findings of a unique lower respiratory transcriptional signature in the days
155 preceding VAP onset, we next asked whether differences in host immune signaling might exist
156 even earlier, two or more weeks before clinical diagnosis of VAP. We hypothesized that such
157 differences might provide insight regarding the increased susceptibility to secondary bacterial
158 infection in these patients.

159 We identified 154 differentially expressed genes at the "early" timepoint **(Table 1)**. The
160 patients who developed VAP exhibited lower expression of several genes with established roles
161 in innate immunity including *IFI30, MMP2, TLR9*, and *DEFB124* **(Figure 3A)**. GSEA further
162 revealed that patients who developed VAP had lower expression of pathways related to
163 antibacterial immune responses including neutrophil degranulation, toll-like receptor signaling, IL-

164 17 signaling, antigen presentation and complement pathways, and higher expression of
165 interferon-alpha/beta signaling pathways, more than two weeks before the onset of VAP **(Figure**
166 **3B)**. Additionally, pathways related to adaptive immunity such as T and B cell receptor signaling
167 were downregulated in the COVID-19 patients who later developed VAP **(Figure 3B)**.

168 To gauge the degree of immune pathway suppression compared to controls, we
169 performed a similar analysis on critically ill intubated patients without infection **(Figure 3C)**.
170 Relative to the control patients, multiple antibacterial immune pathways were downregulated in
171 both COVID-19 groups, with the greatest attenuation in the VAP group **(Figure 3C)**. IPA upstream
172 cytokine analysis predicted reduced activation of multiple proinflammatory cytokines juxtaposed
173 against increased activation of IFNB1 in the VAP patients **(Figure 3D)**. Compared to the control
174 group, the predicted activation states of several proinflammatory cytokines were decreased in
175 both COVID-19 groups **(Figure S2)**.

176 Given prior reports demonstrating a correlation between SARS-CoV-2 viral load and
177 interferon-related gene expression[21] we next asked whether viral load differed between VAP and
178 No-VAP patients. At the "early" timepoint, no differences were observed in either PCR cycle
179 threshold or bulk RNA-seq SARS-CoV-2 reads per million (P=0.53 and P=0.84, respectively)
180 **(Figure S3)**. We also considered the possibility that differences in the number of days of steroid
181 exposure prior to sample collection might explain our findings but found no differences between
182 groups (P=0.34) **(Table S1, S3)**.

183

184 **COVID-19 VAP is associated with impaired antibacterial immune signaling in monocytes**
185 **and macrophages**

186 To further understand the observed downregulation of key antibacterial signaling
187 pathways in COVID-19 patients who developed VAP, we next asked whether this was driven by
188 specific types of immune cells. We performed scRNA-seq on TA specimens and enriched for
189 immune cells using CD45 selection **(Methods)**. We analyzed 12,197 cells from 14 patients after

190 quality control and batch correction. First, we analyzed samples obtained post-intubation at the
191 "early" timepoint. Clustering based upon cellular transcriptional signatures followed by a
192 comparison of cell type proportions did not reveal statistically significant differences between VAP
193 and No-VAP groups with respect to any cell type at the "early" timepoint **(Figure 4A, S4**).
194 Monocytes and macrophages were the most abundant cell types, and thus we focused
195 transcriptional assessment on these two populations.

196 COVID-19 patients who developed VAP had distinct post-intubation transcriptional
197 signatures compared to the No-VAP patients at this "early" timepoint, with respect to the overall
198 monocyte/macrophage cluster **(Figure 4, S4, S5)**. We identified 625 differentially expressed
199 genes (FDR < 0.05) in this cluster and noted downregulation of several genes with key roles in
200 innate immunity in the COVID-19 patients who subsequently developed VAP compared to those
201 who did not, including *IL1Rn, CXCL2, CCL20*, and *JunB*. (**Figure 4C**). In addition, we noted
202 upregulation of interferon-induced genes including *IFI30* and *IFNγR-2*. **(Figure 4C)**. Findings were
203 similar when evaluating differential expression within alveolar macrophages, the largest
204 monocyte/macrophage subset (**Figure S5**).

205 IPA canonical pathway analysis revealed downregulation of several cytokine and innate
206 immune signaling pathways in the patients who later developed VAP at the "early" post-intubation
207 timepoint, including IL-6 and IL-1 signaling, and the NRF2-mediated oxidative stress response
208 (**Figure 4D)**. Computational analysis of upstream cytokine activation predicted impaired activation
209 of multiple pro-inflammatory cytokines in patients who developed VAP, including TNF, IFNγ, and
210 IL1B **(Figure 4E)**. Similar findings were observed in the alveolar macrophage population **(Figure**
211 **S5)**. We were unable to reliably assess the T cell population due to low cell numbers.

212 A comparison of monocytes and macrophages between the VAP and No-VAP patients
213 just prior to VAP onset at the "late" timepoint revealed significant upregulation of genes essential
214 for antibacterial defense. These findings reflected bulk RNA-seq observations and were

215 characterized by upregulation in the VAP group of pathways related to IL-17 and nitric oxide
216 signaling, reactive oxygen species production, and hypercytokinemia **(Figure S6)**.
217
218 **Temporal dynamics of the host response in COVID-19 patients who develop VAP**
219 We next investigated temporal dynamics of the lower airway host immune response in
220 COVID-19 patients from the time of intubation to development of VAP, by evaluating bulk RNA-
221 seq differential gene expression between COVID-19 VAP patients at the "early" timepoint (median
222 of 17 days before VAP onset, n=4) versus "late" timepoint (median of two days before VAP onset,
223 n=5). We identified 2705 differentially expressed genes, and unsupervised hierarchical clustering
224 of the 50 most significant genes demonstrated clear separation of the two timepoints **(Figure 5A)**.
225 GSEA revealed that type I interferon signaling was notably downregulated at the "late" timepoint
226 in comparison to the "early" timepoint **(Figure 5B)**; however, expression of this pathway was still
227 significantly higher in the VAP versus the No-VAP patients **(Figure 2B)**. Several other immune
228 signaling pathways were more highly expressed at the "late" timepoint, presumably reflecting
229 activation of an antibacterial response in the setting of impending bacterial pneumonia **(Figure**
230 **5B)**. Consistent with this, upstream regulator analysis predicted increased activation of several
231 pro-inflammatory cytokines and decreased IFNα and IFNλ signaling at the "late" versus "early"
232 timepoints **(Figure 5C)**.
233 In contrast, comparing No-VAP patients at the "early" (n=8) versus "late" (n=8) timepoints
234 yielded only two genes, both of which were interferon-stimulated genes (*RSAD2* and *CMPK2*)
235 downregulated at the "late" timepoint, suggesting that while the host response was relatively
236 unchanged in these patients, the antiviral response attenuated over time. Indeed, GSEA revealed
237 that type I interferon signaling, and other antiviral immune pathways, were downregulated in the
238 patients who did not develop VAP at the "late" timepoint **(Figure S7)**.
239 We further compared dynamics of host immune responses between VAP and No-VAP
240 patients by performing longitudinal analyses of key immune signaling pathways, including all

241 patients with available bulk RNA-seq samples (VAP: n=7, No-VAP: n=10). Onset of VAP ranged
242 from 10-39 days post intubation (median 19 days), and treatment with immunosuppressants did
243 not differ significantly between comparator groups (p=0.30, Fisher's exact test). Early attenuation
244 of immune signaling in the VAP group was conspicuous, and this pattern eventually resolved later
245 in disease course by the time secondary bacterial infection became established **(Figures 5D-G)**.
246 We confirmed that the observed differences between VAP and No-VAP patients were not driven
247 by differences in treatment with immunosuppressants by comparing pathway Z-scores between
248 patients who received immunosuppressants and those who did not, at the "early" timepoint
249 **(Figure S8)**.
250 We subsequently performed a similar comparison between the "early" and "late"
251 timepoints based on scRNA-seq data from patients who developed VAP. Differential gene
252 expression analysis between these two populations identified 1466 differentially expressed genes
253 in the encompassing monocyte/macrophage cluster. IPA on these genes revealed upregulation
254 of antibacterial signaling pathways at the "late" timepoint, including signaling by several cytokines
255 (including IL-17, IL-6, TNF, IFN) **(Figure 5H-I)**, congruent with the bulk RNA-seq analysis.
256
257 **Lung microbiome disruption precedes VAP in COVID-19 patients**
258 We hypothesized that the innate immune suppression observed in patients who developed
259 VAP would correlate with SARS-CoV-2 viral load. Using TA metatranscriptomics to assess the
260 lower respiratory microbiome, we evaluated longitudinal changes in SARS-CoV-2 abundance.
261 Although no difference in viral load was observed at the "early" timepoint **(Figure S3, Figure 6A)**,
262 the trajectory of SARS-CoV-2 viral load differed significantly in patients who developed VAP. Viral
263 load decreased over time in both groups, however the virus was still detected at later timepoints
264 in patients with VAP, while it was undetected in any of the No-VAP patients at these timepoints
265 (**Figure 6A**). This result suggested that COVID-19 patients who develop VAP may exhibit

266 impaired ability to clear the virus compared to those who do not, and that the lung microbiome
267 composition may be similarly impacted.

268 Indeed, COVID-19 patients who developed VAP exhibited a significant reduction in
269 bacterial alpha diversity of their airway microbiome before clinical signs of infection (Shannon
270 Diversity Index, P=0.0065; **Figure 6B**). Beta diversity did not differ significantly, which may be
271 due to the fact that VAP was caused by different pathogens in each patient, resulting in different
272 airway microbiome compositions in each case **(Figure S9)**. All patients received antibiotics prior
273 to collection of the first sample, suggesting that antibiotic use was not driving these differences
274 **(Table S1)**.

275 We next assessed the most abundant bacterial genera in the lung, as identified by TA
276 metatranscriptomics. At the "early" timepoint, control and No-VAP samples were predominated
277 by common lung commensals, with significant enrichment (FDR < 0.05) of *Alloprevotella*,
278 *Fusobacterium*, and *Neisseria* compared to the VAP group (**Figure 6C**). In the VAP group, early
279 significant enrichment of *Klebsiella* was noted, suggestive of a shift in the microbiome structure
280 that precedes disease onset and culture positive confirmation (**Figure 6C**). By the "late" timepoint,
281 VAP-associated pathogens such as *Citrobacter*, *Escherichia*, and *Klebsiella* were highly
282 prevalent. *Citrobacter* was significantly enriched in VAP versus No-VAP groups at this timepoint,
283 supporting culture results. While highly enriched in VAP, *Klebsiella* did not reach significance at
284 this timepoint due to high variance between individuals (**Figure 6D**). No-VAP patients had a
285 significantly greater abundance of commensal lung microbes, such as *Lactobacillus*,
286 *Bifidobacterium*, and *Veillonella,* at the "late" timepoint **(Figure 6D)**.

287

288 **Discussion**

289 Secondary bacterial pneumonia contributes to significant morbidity and mortality in
290 patients with primary viral lower respiratory tract infections[1,3], but mechanisms governing
291 individual susceptibility to VAP have remained unclear. Few human cohort studies have evaluated

292 the immunologic underpinnings of VAP, and none have been reported in the context of COVID-
293 19, which is characterized by a dysregulated host response distinct from other viral pneumonias[21–
294 23]. To address this gap and probe mechanisms of VAP susceptibility in patients with COVID-19,
295 we carried out a systems biological assessment of host and microbial dynamics of the lower
296 respiratory tract.

297 Two days before VAP onset, a transcriptional signature consistent with bacterial infection
298 was observed. This finding suggests that host response changes can occur before clinical
299 recognition of pneumonia, highlighting the potential utility of the host transcriptome as a tool for
300 VAP surveillance. While intriguing, this observation did not provide an explanation for differential
301 susceptibility of some COVID-19 patients to post-viral pneumonia.

302 The discovery of an early suppressed antibacterial immune response in patients who later
303 developed VAP did, however, offer a potential explanation. More than two weeks before VAP
304 onset, we observed a striking suppression of pathways related to both innate and adaptive
305 immunity, including neutrophil degranulation, toll-like receptor (TLR) signaling, complement
306 activation, antigen presentation, and T cell receptor and B receptor signaling, as well as signaling
307 by several cytokines (e.g. IL-1, IL-4, IL-12, IL-13 and IL-17). Comparison against uninfected,
308 intubated controls confirmed the previously described paradoxical impairment in immune
309 signaling found in patients with severe COVID-19[22], and suggested that VAP susceptibility may
310 be the result of disproportionate suppression of innate and adaptive pathways critical for
311 antibacterial defense, resulting in enhanced susceptibility to opportunistic secondary infections.

312 Animal models of influenza have provided insight into potential mechanisms of post-viral
313 pneumonia, although none have provided insight regarding why some individuals are more
314 susceptible than others. In mice inoculated with influenza, for instance, virus-induced type I
315 interferon suppresses neutrophil chemokines and impairs Th17 immunity, compromising effective
316 clearance of bacterial infections[10,11]. Interestingly, we also observed increased type I interferon
317 signaling in COVID-19 patients who weeks later developed VAP, and an impairment in IL-17

318 signaling and other immune pathways. Desensitization to TLR ligands after influenza infection
319 has also been documented[24], which is congruent with the downregulation of TLR signaling at the
320 time of intubation observed in our bulk RNA-seq analyses.

321 We asked whether certain cell types were responsible for driving the early suppression of
322 immune signaling observed in COVID-19 patients who went on to develop VAP. No significant
323 differences in proportions of any cell types was observed between patients with or without VAP
324 at the time of intubation. This finding suggests that an impairment of immune cell recruitment was
325 not causing these differences, but rather significant gene expression differences within these
326 immune cell populations.

327 In the most predominant cell population, the monocytes and macrophages, we observed
328 broad downregulation of the innate and adaptive immune responses, concordant with global
329 observations in bulk RNA-seq analyses. Further, we noted a downregulation of key pathways
330 involved in antimicrobial immune responses including TREM1, IL-1, and IL-6 signaling. Overall,
331 our data suggest that while no difference in cell type populations existed between groups,
332 changes in the gene expression within monocytes and macrophages contributes to immune
333 suppression in COVID-19 patients who later develop VAP.

334 SARS-CoV-2 viral load correlates with interferon stimulated gene expression[21,22] and thus
335 we initially hypothesized that differences in viral load between groups might relate to individual
336 VAP susceptibility. However, we found no difference between groups at the “early” timepoint.
337 Moreover, no differences existed in terms of immunosuppressive medication administration or
338 clinically diagnosed immunodeficiency, suggesting that other, still unidentified mechanisms
339 present at the time of intubation must underlie the marked suppression of immune gene
340 expression in COVID-19 patients who went on to develop VAP.

341 While no difference in viral load was observed at the time of intubation, the COVID-19
342 patients who developed VAP exhibited impaired viral clearance over the time-course of intubation.
343 This observation was corroborated by a prolonged antiviral type I interferon response at the “late”

344 timepoint (median of two days before VAP onset) in patients who developed VAP versus those
345 who did not, pointing to the persistence of suboptimal antiviral immunity in these patients. Early
346 induction of functional SARS-CoV-2 specific T cells is associated with faster viral clearance in
347 COVID-19 patients[25] and likewise, we observed impairments in T cell activation and signaling in
348 the VAP group by bulk RNA-seq at the "early" timepoint, which further suggests a decreased
349 ability to control the virus in these patients.

350 Respiratory viruses can reshape the human airway microbiome by modulating host
351 inflammatory responses[26,27]. In mouse models of influenza, the airway microbiome exhibits
352 expansion of several bacterial families during the course of viral infection as innate immunity is
353 suppressed[26]. These changes increase the risk of secondary bacterial infection[26] and have been
354 observed in patients with chronic obstructive pulmonary disease, where suppression of the innate
355 immune response in rhinovirus infected patients may be followed by bacterial superinfection[28,29].

356 Similarly, the innate immune suppression observed in COVID-19 patients who developed
357 VAP was associated with airway microbiome collapse and the outgrowth of lung pathogens in
358 advance of clinical VAP diagnosis. This finding suggests that individual immune responses to
359 SARS-CoV-2 infection may drive a restructuring of the microbial community and increase
360 susceptibility to VAP (**Figure 7**). The resulting outgrowth of a VAP-associated bacterial pathogen
361 may elicit an antibacterial response, but the broader immunosuppressive state preceding this
362 response may be insufficient to control the development of clinical pneumonia. Those with a
363 lesser degree of immunosuppression may be able to respond faster and therefore control
364 opportunistic bacterial pathogens more effectively.

365 These findings may also have important implications for management of patients with
366 COVID-19 related acute respiratory failure, many of whom are now being treated with
367 corticosteroids and other immunosuppressive drugs. These agents may lead to further
368 suppression of the key pathways required for host response to secondary bacterial infection.
369 Thus, our results emphasize the need for ongoing vigilance for VAP in patients treated with potent

370 immunosuppressive agents, as well as the need to develop novel diagnostic and/or prognostic
371 approaches to identifying patients at highest risk.

372 Protein biomarkers of immune function have been associated with nosocomial infection in
373 critically ill patients[15], although not in the context of viral infection. Further studies with a larger
374 cohort may allow for the identification of transcriptomic biomarkers to assess a COVID-19
375 patient's risk of VAP at the time of intubation, which could reduce inappropriate use of prophylactic
376 antibiotics or immunomodulatory treatments, or signal a need for enhanced surveillance
377 strategies.

378 Sample size is a limitation of this study, which could result in over-fitting to this small set
379 of patients; however, the reproducibility of our observations across both bulk and scRNA-seq
380 analyses and the significant number of differentially expressed genes among the comparator
381 groups support the internal validity of our conclusions. Additional studies in a larger independent
382 cohort will be needed to determine the utility of lower respiratory gene expression biomarkers for
383 predicting future development of VAP. Because this study was limited to critically ill, intubated
384 patients, we were unable to assess early stages of COVID-19, which may provide additional
385 insight regarding determinants of secondary bacterial infection.

386 We were unable to assess whether epithelial cells contributed to VAP risk due to
387 enrichment for immune cells prior to scRNA-seq. However, given that monocytes, macrophages
388 and lymphocytes can both be infected by SARS-CoV-2 and contribute to disease pathophysiology
389 and resolution[30–32], our findings are apropos. With larger cohorts, the early detection of specific
390 immune pathway suppression and microbiome collapse could be leveraged to develop clinically
391 useful models for identifying COVID-19 patients with increased susceptibility to secondary
392 bacterial pneumonia.

393

394 **Materials and Methods**

395

396 **Study design, cohorts, and enrollment**

397 We conducted a prospective case-control study of adults requiring mechanical ventilation
398 for COVID-19 with or without secondary bacterial pneumonia. We also evaluated control patients
399 requiring mechanical ventilation for other reasons who had no evidence of pulmonary infection
400 (**Figure 1**). Patients were enrolled in either of two prospective cohort studies of critically ill patients
401 at the University of California, San Francisco (UCSF) and Zuckerberg San Francisco General
402 Hospital between 07/2013 and 07/2020[33]. Of the COVID-19 patients, 17 were co-enrolled in the
403 National Institute of Allergy and Infectious Diseases-funded Immunophenotyping Assessment in
404 a COVID-19 Cohort (IMPACC) Network study.

405

406 **Ventilator-associated pneumonia adjudication**

407 A total of 63 adults who required intubation for severe COVID-19 (Cohort 1) and who had
408 available TA samples were considered for inclusion in the study (**Figure 1**). Patients who met the
409 US Centers for Disease Control (CDC) definition for VAP[20] (based on the PNU1 and PNU2
410 definitions) and had a positive bacterial respiratory culture were adjudicated as having VAP for
411 the purpose of the study (n=16). Patients who did not meet these criteria, and for whom there was
412 no sustained clinical suspicion for bacterial pneumonia during the admission, were categorized
413 as No-VAP (n=17).

414 VAP and No-VAP patients for whom samples at the timepoints of interest were available
415 were included in the analyses (VAP: n=10; No-VAP: n=13). Patients who met CDC-VAP criteria
416 but had negative TA cultures (n=5 patients), as well as patients with clinically suspected bacterial
417 pneumonia who did not meet CDC VAP criteria and had a positive (n=6) or negative (n=5) TA
418 culture were excluded. Fourteen patients who met clinical pneumonia criteria on intubation were
419 also excluded. Eight intubated patients from a recent study[22] (Cohort 2) were included as controls
420 and were selected because they had previously been adjudicated as having no evidence of lower
421 respiratory tract infection. This group included four patients with acute respiratory distress

422 syndrome (ARDS) due to non-infectious etiologies, and four patients without ARDS who were
423 intubated for other reasons (subdural hematoma (n=1), retroperitoneal hemorrhage (n=1), or
424 neurosurgical procedures (n=2)).
425
426 **Tracheal aspirate sampling**
427 Following enrollment, tracheal aspirate (TA) was collected (periodically following
428 intubation for Study 1, or once within three days of intubation for Study 2), without addition of
429 saline wash, and either a) mixed 1:1 with DNA/RNA shield (Zymo Research) for bulk RNA-seq or
430 b) immediately processed in a biosafety level 3 laboratory (BSL3) for scRNA-seq analysis.
431 **Bulk RNA sequencing and host transcriptome analysis**
432
433 RNA sequencing
434 To evaluate host and microbial gene expression, metatranscriptomic next generation RNA
435 sequencing (RNA-seq) was performed on TA specimens. Following RNA extraction (Zymo
436 Pathogen Magbead Kit) and DNase treatment, human cytosolic and mitochondrial ribosomal RNA
437 was depleted using FastSelect (Qiagen). To control for background contamination, we included
438 negative controls (water and HeLa cell RNA) as well as positive controls (spike-in RNA standards
439 from the External RNA Controls Consortium (ERCC))[34]. RNA was then fragmented and
440 underwent library preparation using the NEBNext Ultra II RNA-seq Kit (New England Biolabs).
441 Libraries underwent 146 nucleotide paired-end Illumina sequencing on an Illumina Novaseq 6000.
442
443 Host differential expression
444 Following demultiplexing, sequencing reads were pseudo-aligned with kallisto[35] to an
445 index consisting of all transcripts associated with human protein coding genes (ENSEMBL v. 99),
446 cytosolic and mitochondrial ribosomal RNA sequences and the sequences of ERCC RNA
447 standards. Gene-level counts were generated from the transcript-level abundance estimates

448 using the R package tximport[36], with the scaledTPM method. Samples retained in the dataset had
449 a total of at least 1,000,000 estimated counts associated with transcripts of protein coding genes.
450 Genes were retained for differential expression analysis if they had counts in at least 30%
451 of samples. Differential expression analysis was performed using the R package DESeq2[37]. We
452 modeled the expression of individual genes using the design formula ~VAPgroup, where VAP
453 groups were "VAP-early", "No-VAP-early", "VAP-late" and "No-VAP-late" and used the results()
454 function to extract a specific contrast. Separate comparisons to the control group were performed
455 using the design formula ~COVID-19-status to compare positive and negative patients.
456 Significant genes were identified using a Benjamini-Hochberg false discovery rate (FDR)
457 < 0.1. We generated heatmaps of the top 50 differentially expressed genes by FDR. For
458 visualization, gene expression was normalized using the regularized log transformation, centered,
459 and scaled prior to clustering. Heatmaps were generated using the *pheatmap* package. Columns
460 were clustered using Euclidean distance and rows were clustered using Pearson correlation.
461 Differential expression analysis results are provided in (**Supplementary Data File 1**).
462
463 Pathway analysis
464 Gene set enrichment analyses (GSEA) were performed using the fgseaMultilevel function
465 in the R package fgsea[38] and REACTOME[39] pathways with a minimum size of 10 genes and a
466 maximum size of 1,500 genes. All genes were included in the comparison, pre-ranked by the test
467 statistic. Significant pathways were defined as those with a Benjamini-Hochberg adjusted P-value
468 < 0.05. Ingenuity Pathway Analysis (IPA) Canonical Pathway and Upstream Regulator Analysis[40]
469 was employed on genes with P < 0.1 and ranked by the test statistic to identify cytokine regulators.
470 Significant IPA results were defined as those with a Z-score absolute value greater than 2 and an
471 overlap P-value < 0.05. The gene sets in figures were selected to reduce redundancy and
472 highlight diverse biological functions. Full GSEA and IPA results are provided in (**Supplementary**
473 **Data Files 2 and 3**).

474 Longitudinal pathway analysis was performed using all available TA samples spanning
475 post-intubation to VAP onset for all patients included in the bulk RNA-seq analysis. Analysis was
476 restricted to samples with at least 1,000,000 human protein coding transcripts. Pathways of
477 interest were selected from the significant GSEA results of the comparison of VAP vs. No-VAP
478 patients in the "early" timepoint. The top 20 leading edge genes were selected from each pathway
479 for analysis. To calculate a Z-score for each gene, expression was normalized using the variance
480 stabilizing transformation (VST), centered, and scaled. A pathway Z-score was calculated by
481 averaging the 20 gene Z-scores. Multiple Z-scores per patient at a given time interval were
482 averaged so that each patient corresponds to one datapoint at each interval. Statistical
483 significance of pathway expression over time between VAP and No-VAP groups was calculated
484 using a two-way analysis of variance (ANOVA) in GraphPad PRISM.
485
486 **Single cell RNA sequencing and transcriptome analysis**
487 After collection, fresh TA was transported to a BSL-3 laboratory at ambient temperature
488 to improve neutrophil survival. 3mL of TA was dissociated in 40mL of PBS with 50ug/mL
489 collagenase type 4 (Worthington) and 0.56 ku/mL of Dnase I (Worthington) for 10 minutes at room
490 temperature, followed by passage through a 70μM filter. Cells were pelleted at 350g 4C for 10
491 minutes, resuspended in PBS with 2mM EDTA and 0.5% BSA, and manually counted on a
492 hemocytometer. Cells were stained with MojoSort Human CD45 and purified by the
493 manufacturer's protocol (Biolegend). After CD45 positive selection, cells were manually counted
494 with trypan blue on a hemocytometer. Using a V(D)J v1.1 kit according to the manufacturer's
495 protocol, samples were loaded on a 10X Genomics Chip A without multiplexing, aiming to capture
496 10,000 cells (10X Genomics). Libraries underwent paired end 150 base pair sequencing on an
497 Illumina NovaSeq6000.
498 Raw sequencing reads were aligned to GRCh38 using the STAR aligner . Cell barcodes
499 were then determined based upon UMI count distribution. Read count matrices were generated

500 through the 10X genomics cellranger pipeline v3.0. Data was processed and analyzed using the
501 Scanpy v1.6[42]. Cells that had <200 genes, <20% mitochondrial reads, and had greater than 2500
502 counts were filtered. Mitochondrial genes were removed and multi-sample integration was
503 performed using single-cell variational inference (scVI)[43]. Differential expression was performed
504 using MAST v1.16.0[44]. Differential expression analysis results are detailed in (**Supplementary**
505 **Data File 4**).
506
507 Pathway analysis
508 Ingenuity Pathway Analysis (IPA) Canonical Pathway and Upstream Regulator Analysis[40]
509 was employed on genes with $P < 0.05$ and ranked by log2foldchange to identify canonical
510 pathways and cytokine regulators. Due to the significantly greater number of differentially
511 expressed genes in scRNA-seq analyses, we utilized a more restrictive cutoff of $FDR < 0.05$ for
512 scRNA-seq to ensure a similar number of genes were input into IPA. Significant IPA results were
513 defined as those with a Z-score absolute value greater than 2 and an overlap P-value < 0.05. The
514 gene sets in figures were selected to reduce redundancy and highlight diverse biological
515 functions. Full GSEA and IPA results are provided in (**Supplementary Data Files 5 and 6**).
516
517 **Lung microbiome analysis**
518 RNA from tracheal aspirates was sequenced as described above. Taxonomic alignments
519 were obtained from raw sequencing reads using the IDseq pipeline[45,46], which performs quality
520 filtration and removal of human reads followed by reference-based taxonomic alignment at both
521 the nucleotide and amino acid level against sequences in the National Center for Biotechnology
522 Information (NCBI) nucleotide (NT) and non-redundant (NR) databases, followed by assembly of
523 reads matching each taxon detected. Taxonomic alignments underwent background correction
524 for environmental contaminants (see below), viruses were excluded, and data was then
525 aggregated to the genus level before calculating diversity metrics. Alpha diversity (Shannon's

526 Diversity Index) and beta diversity (Bray-Curtis dissimilarity) were calculated and the latter plotted
527 using non-metric multidimensional scaling (NDMS). Comparison of alpha and beta diversity over
528 time between VAP and No-VAP groups was calculated using a two-way analysis of variance
529 (ANOVA) in R. Top ten taxa in each group were identified by ranking the percent of counts for
530 each genus among total bacterial counts in each group. Significantly enriched taxa were
531 evaluated by comparing distributions using three models (Poisson, negative binomial, and zero-
532 inflated negative binomial mixed-effects models) and correcting for multiple hypothesis testing
533 using Benjamini-Hochberg as previously described[47]. Significantly enriched taxa were called
534 using a $q < 0.05$ cutoff.
535
536 Identification and mitigation of environmental contaminants
537 To minimize inaccurate taxonomic assignments due to environmental and reagent derived
538 contaminants, non-templated "water only" and HeLa cell RNA controls were processed with each
539 group of samples that underwent nucleic acid extraction. These were included, as well as positive
540 control clinical samples, with each sequencing run. Negative control samples enabled estimation
541 of the number of background reads expected for each taxon. A previously developed negative
542 binomial model[21] was employed to identify taxa with NT sequencing alignments present at an
543 abundance significantly greater compared to negative water controls. This was done by modeling
544 the number of background reads as a negative binomial distribution, with mean and dispersion
545 fitted on the negative controls. For each batch (sequencing run) and taxon, we estimated the
546 mean parameter of the negative binomial by averaging the read counts across all negative
547 controls, slightly regularizing this estimate by including the global average (across all batches) as
548 an additional sample. We estimated a single dispersion parameter across all taxa and batches,
549 using the functions glm.nb() and theta.md() from the R package MASS[48]. Taxa that achieved a
550 P-value < 0.01 were carried forward.
551

552 **Statistics**

553 Statistical significance was defined as $P < 0.05$, using two-tailed tests. Categorical data were
554 analyzed by Fisher's exact test and nonparametric continuous variables were analyzed by Mann-
555 Whitney. Statistical approaches used for gene expression and microbiome analyses are detailed
556 in each respective Methods section.

557

558 **Study approval**

559 Both cohort studies were approved by the UCSF Institutional Review Board (IRB) under
560 protocols 10-02701 (control patients, pre-COVID-19 pandemic) and 20-30497 (COVID-19
561 patients, COVID-19 Multiphenotyping for Effective Therapy (COMET) study), respectively.
562 Detailed enrollment and consent protocols for both studies have been previously described[18,33].

563

564 **References**

565 1. Falsey, A. R. *et al.* Bacterial Complications of Respiratory Tract Viral Illness: A
566 Comprehensive Evaluation. *The Journal of Infectious Diseases* **208**, 432–441 (2013).
567 2. Morens, D. M., Taubenberger, J. K. & Fauci, A. S. Predominant role of bacterial pneumonia
568 as a cause of death in pandemic influenza: implications for pandemic influenza
569 preparedness. *J Infect Dis* **198**, 962–970 (2008).
570 3. Rouzé, A. *et al.* Relationship between SARS-CoV-2 infection and the incidence of ventilator-
571 associated lower respiratory tract infections: a European multicenter cohort study. *Intensive*
572 *Care Med* 1–11 (2021) doi:10.1007/s00134-020-06323-9.
573 4. DeVoe, C. *et al.* Increased Rates of Secondary Bacterial Infections, Including Enterococcus
574 Bacteremia, in Patients Hospitalized with COVID-19. *Infect Control Hosp Epidemiol* 1–33
575 (2021) doi:10.1017/ice.2021.391.
576 5. Luyt, C.-E. *et al.* Ventilator-associated pneumonia in patients with SARS-CoV-2-associated
577 acute respiratory distress syndrome requiring ECMO: a retrospective cohort study. *Ann*
578 *Intensive Care* **10**, 158 (2020).
579 6. Bardi, T. *et al.* Nosocomial infections associated to COVID-19 in the intensive care unit:
580 clinical characteristics and outcome. *Eur J Clin Microbiol Infect Dis* (2021)
581 doi:10.1007/s10096-020-04142-w.
582 7. Maes, M. *et al.* Ventilator-associated pneumonia in critically ill patients with COVID-19. *Crit*
583 *Care* **25**, 25 (2021).
584 8. Søgaard, K. K. *et al.* Community-acquired and hospital-acquired respiratory tract infection
585 and bloodstream infection in patients hospitalized with COVID-19 pneumonia. *J Intensive*
586 *Care* **9**, (2021).
587 9. Metzger, D. W. & Sun, K. Immune Dysfunction and Bacterial Co-Infections following
588 Influenza. *J Immunol* **191**, 2047–2052 (2013).

589 10. Shahangian, A. *et al.* Type I IFNs mediate development of postinfluenza bacterial
590 pneumonia in mice. *J Clin Invest* **119**, 1910–1920 (2009).
591 11. Kudva, A. *et al.* Influenza A inhibits Th17-mediated host defense against bacterial
592 pneumonia in mice. *J Immunol* **186**, 1666–1674 (2011).
593 12. Boxx, G. M. & Cheng, G. The Roles of Type I Interferon in Bacterial Infection. *Cell Host*
594 *Microbe* **19**, 760–769 (2016).
595 13. Pelekanou, A. *et al.* Decrease of CD4-lymphocytes and apoptosis of CD14-monocytes are
596 characteristic alterations in sepsis caused by ventilator-associated pneumonia: results from
597 an observational study. *Crit Care* **13**, R172 (2009).
598 14. Wunderink, R. G. Nosocomial Pneumonia, Including Ventilator-associatedPneumonia. *Proc*
599 *Am Thorac Soc* **2**, 440–444 (2005).
600 15. Conway Morris, A. *et al.* Cell-surface signatures of immune dysfunction risk-stratify critically
601 ill patients: INFECT study. *Intensive Care Med* **44**, 627–635 (2018).
602 16. Ballinger, M. N. & Standiford, T. J. Innate Immune Responses in Ventilator-Associated
603 Pneumonia. in *Mucosal Immunology of Acute Bacterial Pneumonia* (ed. Prince, A.) 185–212
604 (Springer New York, 2013). doi:10.1007/978-1-4614-5326-0_8.
605 17. Kalil, A. C. *et al.* Management of Adults With Hospital-acquired and Ventilator-associated
606 Pneumonia: 2016 Clinical Practice Guidelines by the Infectious Diseases Society of America
607 and the American Thoracic Society. *Clin Infect Dis* **63**, e61–e111 (2016).
608 18. Langelier, C. *et al.* Integrating host response and unbiased microbe detection for lower
609 respiratory tract infection diagnosis in critically ill adults. *Proc Natl Acad Sci U S A* **115**,
610 E12353–E12362 (2018).
611 19. Flanagan, J. L. *et al.* Loss of bacterial diversity during antibiotic treatment of intubated
612 patients colonized with Pseudomonas aeruginosa. *J Clin Microbiol* **45**, 1954–1962 (2007).
613 20. CDC-NHSN. Pneumonia (Ventilator-associated [VAP] and non-ventilator-associated
614 Pneumonia [PNEU]) Event.

615 21. Mick, E. *et al.* Upper airway gene expression reveals suppressed immune responses to
616 SARS-CoV-2 compared with other respiratory viruses. *Nature Communications* **11**, 5854
617 (2020).
618 22. Sarma, A. *et al.* COVID-19 ARDS is characterized by a dysregulated host response that
619 differs from cytokine storm and is modified by dexamethasone. *Res Sq* (2021)
620 doi:10.21203/rs.3.rs-141578/v1.
621 23. Blanco-Melo, Daniel. Imbalanced host response to SARS-CoV-2 drives development of
622 COVID-19. *Cell.* doi:10.1016/j.cell.2020.04.026.
623 24. Didierlaurent, A. *et al.* Sustained desensitization to bacterial Toll-like receptor ligands after
624 resolution of respiratory influenza infection. *J Exp Med* **205**, 323–329 (2008).
625 25. Tan, A. T. *et al.* Early induction of functional SARS-CoV-2-specific T cells associates with
626 rapid viral clearance and mild disease in COVID-19 patients. *Cell Reports* **34**, 108728
627 (2021).
628 26. Goulding, J. *et al.* Lowering the Threshold of Lung Innate Immune Cell Activation Alters
629 Susceptibility to Secondary Bacterial Superinfection. *J Infect Dis* **204**, 1086–1094 (2011).
630 27. Man, W. H., de Steenhuijsen Piters, W. A. A. & Bogaert, D. The microbiota of the respiratory
631 tract: gatekeeper to respiratory health. *Nat Rev Microbiol* **15**, 259–270 (2017).
632 28. Mallia, P. *et al.* Rhinovirus Infection Induces Degradation of Antimicrobial Peptides and
633 Secondary Bacterial Infection in Chronic Obstructive Pulmonary Disease. *Am J Respir Crit*
634 *Care Med* **186**, 1117–1124 (2012).
635 29. Molyneaux, P. L. *et al.* Outgrowth of the Bacterial Airway Microbiome after Rhinovirus
636 Exacerbation of Chronic Obstructive Pulmonary Disease. *Am J Respir Crit Care Med* **188**,
637 1224–1231 (2013).
638 30. The NU SCRIPT Study Investigators *et al.* Circuits between infected macrophages and T
639 cells in SARS-CoV-2 pneumonia. *Nature* **590**, 635–641 (2021).

640 31. Borsa, M. & Mazet, J. M. Attacking the defence: SARS-CoV-2 can infect immune cells. *Nat*
641 *Rev Immunol* **20**, 592–592 (2020).
642 32. Boumaza, A. *et al.* Monocytes and Macrophages, Targets of Severe Acute Respiratory
643 Syndrome Coronavirus 2: The Clue for Coronavirus Disease 2019 Immunoparalysis. *J Infect*
644 *Dis* **224**, 395–406 (2021).
645 33. Sarma, A. *et al.* Tracheal aspirate RNA sequencing identifies distinct immunological
646 features of COVID-19 ARDS. *Nat Commun* **12**, 5152 (2021).
647 34. Pine, P. S. *et al.* Evaluation of the External RNA Controls Consortium (ERCC) reference
648 material using a modified Latin square design. *BMC Biotechnol* **16**, 54 (2016).
649 35. Bray, N. L., Pimentel, H., Melsted, P. & Pachter, L. Near-optimal probabilistic RNA-seq
650 quantification. *Nature Biotechnology* **34**, 525–527 (2016).
651 36. Soneson, C., Love, M. I. & Robinson, M. D. Differential analyses for RNA-seq: transcript-
652 level estimates improve gene-level inferences. *F1000Res* **4**, 1521 (2015).
653 37. Love, M. I., Huber, W. & Anders, S. Moderated estimation of fold change and dispersion for
654 RNA-seq data with DESeq2. *Genome Biol* **15**, 550 (2014).
655 38. Korotkevich, G., Sukhov, V. & Sergushichev, A. Fast gene set enrichment analysis. *bioRxiv*
656 060012 (2019) doi:10.1101/060012.
657 39. Croft, D. *et al.* The Reactome pathway knowledgebase. *Nucleic Acids Res* **42**, D472-477
658 (2014).
659 40. Krämer, A., Green, J., Pollard, J. & Tugendreich, S. Causal analysis approaches in
660 Ingenuity Pathway Analysis. *Bioinformatics* **30**, 523–530 (2014).
661 41. Dobin, A. *et al.* STAR: ultrafast universal RNA-seq aligner. *Bioinformatics* **29**, 15–21 (2013).
662 42. Wolf, F. A., Angerer, P. & Theis, F. J. SCANPY : large-scale single-cell gene expression
663 data analysis. *Genome Biology* **19**, 15 (2018).
664 43. Lopez, R., Regier, J., Cole, M. B., Jordan, M. I. & Yosef, N. Deep Generative Modeling for
665 Single-cell Transcriptomics. *Nat Methods* **15**, 1053–1058 (2018).

666 44. Finak, G. *et al.* MAST: a flexible statistical framework for assessing transcriptional changes
667 and characterizing heterogeneity in single-cell RNA sequencing data. *Genome Biol* **16**, 278
668 (2015).
669 45. Ramesh, A. *et al.* Metagenomic next-generation sequencing of samples from pediatric
670 febrile illness in Tororo, Uganda. *PLoS One* **14**, e0218318 (2019).
671 46. Kalantar, K. L. *et al.* IDseq—An open source cloud-based pipeline and analysis service for
672 metagenomic pathogen detection and monitoring. *Gigascience* **9**, (2020).
673 47. Durack, J. *et al.* Delayed gut microbiota development in high-risk for asthma infants is
674 temporarily modifiable by Lactobacillus supplementation. *Nat Commun* **9**, 707 (2018).
675 48. Venables, W. N. & Ripley, B. D. *Modern Applied Statistics with S*. (Springer-Verlag, 2002).
676 doi:10.1007/978-0-387-21706-2.
677
678

679 Author contributions:

680 Conceptualization: CRL, AT, BSZ, AB, CD, SL, ER, AP, OR, CSC

681 Methodology: CRL, AT, BSZ, AB, CD, SL, ER, AJT, OR

682 Data acquisition: RG, AJ, PHS, TJD, BSZ, AB, NGJ, AD

683 Formal analysis: AT, BSZ, AB, CD, SL, ER, AJT, EM, JA

684 Investigation: BSZ, AB, CD, SS, CSC, DJE

685 Funding acquisition: CRL, CSC, JLD, DJE

686 Supervision: CRL, OR, NN, JLD, CSC, DJE

687 Writing - original draft: AT, BSZ, AB, CD, SL, ER, CRL

688 Writing - review & editing: All authors

689

690 Acknowledgements: This study was performed with support from the National Institute of Allergy

691 and Infectious Diseases-sponsored Immunophenotyping Assessment in a COVID-19 Cohort

692 (IMPACC) Network. We gratefully appreciate support from Amy Kistler, PhD, Jack Kamm, PhD,

693 Saharai Caldera, BS and Maira Phelps BS.

694

695 Funding: Funding for the COMET cohort enrollment, sample collection and data analysis derived

696 from: K23HL138461-01A1 (CL), K24HL137013 (PGW), F32 HL151117 (AS), R35 HL140026

697 (CSC), NIAID U19AI077439 (DJE), Chan Zuckerberg Biohub (AB, JLD). The UCSF IMPACC site

698 was funded by NIAID U19AI077439 (DJE). Funding for enrollment of COMET participants not

699 enrolled in IMPACC and for all sample collection and data analysis derived from K23HL138461-

700 01A1 (CL), K24HL137013 (PGW), F32 HL151117 (AS), R35 HL140026 (CSC), and the Chan

701 Zuckerberg Biohub (AB, JLD). Philanthropic support was provided from Mark and Carrie Casey,

702 Julia and Kevin Hartz, Carl Kawaja and Wendy Holcombe, Eric Keisman and Linda Nevin, Martin

703 and Leesa Romo, Three Sisters Foundation, Diana Wagner and Jerry Yang and Akiko Yamazaki.

704

705 Data and materials availability: Host gene expression data are available under NCBI GEO
706 accession number GSE168019 for bulk RNA-seq and GSE168018 for scRNA-seq. Raw microbial
707 sequencing alignments are available from NCBI SRA under BioProject PRJNA704082. Code
708 used for RNA-seq and microbiome analyses is available at
709 https://github.com/bspeco/VAPinCOVID19.

710 **Table 1**: Clinical characteristics of patients with COVID-19 who do or do not develop VAP at the
711 "early" and "late" timepoints. Additional clinical and demographic characteristics can be found in
712 Supplementary Tables 1 (bulk RNA-seq) and 2 (single cell RNA-seq).
713

	VAP (early timepoint)	No-VAP (early timepoint)	P-value (early - VAP vs No-VAP)	VAP (late timepoint)	No-VAP (late timepoint)	P-value (late - VAP vs No-VAP)	Controls (early timepoint)	P-value (+/- COVID-19)
Bulk RNA-seq								
N	4	8		5	8		8	
Age, median (IQR)	59.5 (56.0, 66.0)	49 (40.5, 64.0)	0.268	51.0 (48.0, 53.0)	59.5 (47.0, 64.5)	0.271	63.0 (36.0, 79.0)	0.642
Female (%)	1 (25.0%)	3 (37.5%)	1.00	2 (40.0%)	4 (50.0%)	1.00	4 (50.0%)	0.648
Days before VAP (median [range])	16.5 (15, 38)	-	-	2 (2, 3)	-	-	-	-
Days post intubation (median [range])	2 (1, 5)	2 (1, 4)	0.930	17 (8, 23)	9 (6, 19)	0.160	1 (1, 3)	0.062
Cultured microbe in VAP patients (n)								
Klebsiella aerogenes	2	-	-	2	-	-	-	-
Staphylococcus aureus	1	-	-	0	-	-	-	-
Proteus mirabilis	1	-	-	1	-	-	-	-
Citrobacter koserii	0	-	-	1	-	-	-	-
Serratia marcescens	0	-	-	1	-	-	-	-
Pseudomonas aeruginosa	0	-	-	0	-	-	-	-
Single cell RNA-seq								
N	4	6		4	4		-	-
Age, median (IQR)	64.0 (50.5, 76.5)	56.5 (47.0, 68.0)	0.392	61.5 (37.5, 74.0)	60.0 (50.5, 74.0)	0.271	-	-
Female (%)	2 (50.0%)	2 (33.3%)	1.00	0 (0.0%)	2 (50.0%)	0.429	-	-
Days before VAP, median (range)	9.5 (8, 16)	-	-	3 (2, 4)	-	-	-	-
Days after intubation, median (range)	5.5 (1, 10)	4 (2, 13)	0.748	8.5 (7, 18)	10.5 (4, 15)	0.884	-	-
Cultured microbe in VAP patients (n)								-
Staphylococcus aureus	1	-	-	0	-	-	-	-
Klebsiella aerogenes	1	-	-	1	-	-	-	-
Citrobacter koserii	1	-	-	1	-	-	-	-
Proteus mirabilis	0	-	-	0	-	-	-	-
Serratia marcescens	0	-	-	1	-	-	-	-
Pseudomonas aeruginosa	1	-	-	1	-	-	-	-

714
715 Statistical significance was determined using Fisher's exact test (categorical variables) or by Wilcoxon test (continuous variables).
716 Abbreviations: IQR: interquartile range; VAP: ventilator-associated pneumonia.
717
718

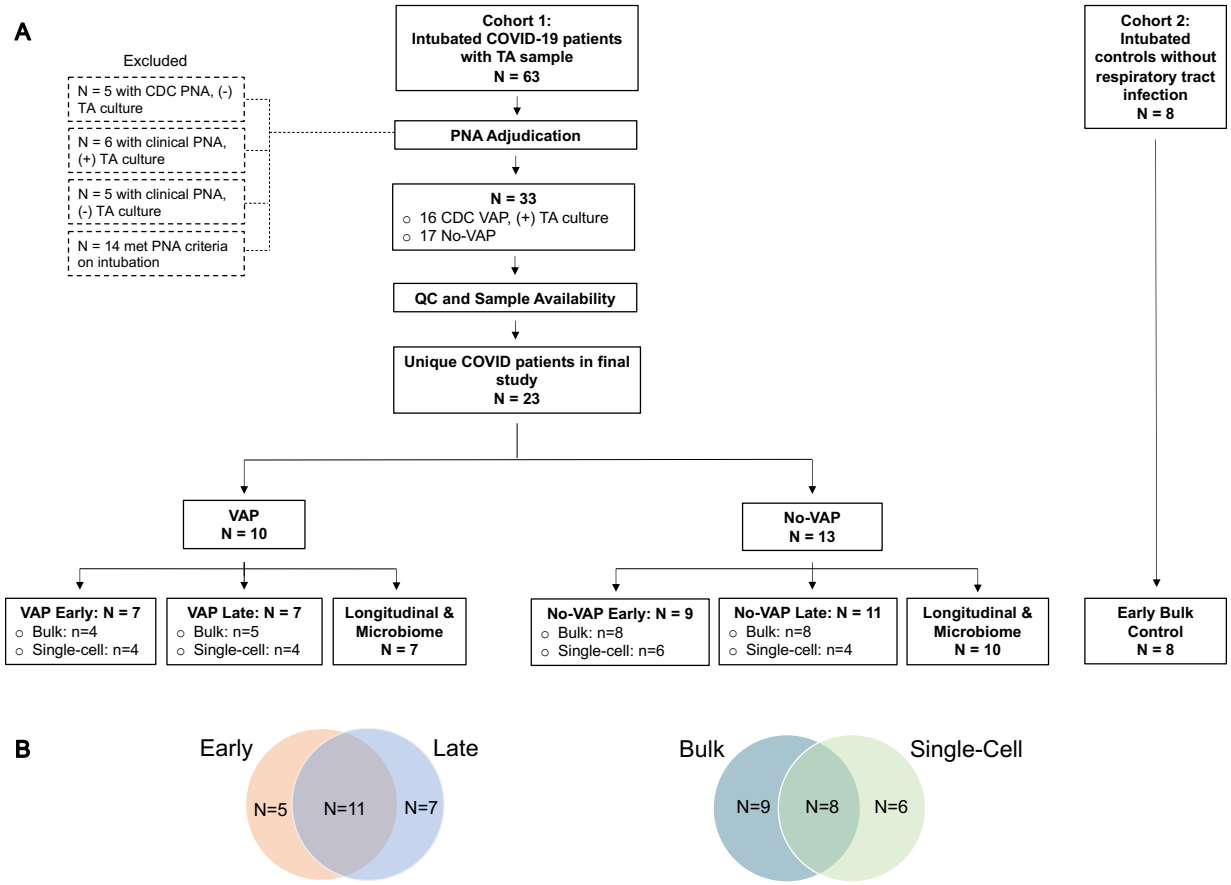

Figure 1: Study flowchart.
A) Two patient cohorts were studied. Cohort 1 consisted of COVID-19 patients from the COVID Multiphenotyping for Effective Therapies (COMET) / Immunophenotyping Assessment in a COVID-19 Cohort (IMPACC) studies (described in Methods). Cohort 2 consisted of critically ill intubated control patients from a prior prospective cohort study led by our research group[22]. The "early" samples were the first available tracheal aspirate specimens after intubation, and for the VAP group were collected >7 days prior to VAP onset. The "late" samples were obtained 2-4 days before VAP onset for the VAP group; for the No-VAP group, samples were selected to match the VAP group's time from intubation as closely as possible. Controls included eight critically ill, mechanically ventilated patients without LRTI. All COVID-19 patients included in the primary bulk analysis were also included in the longitudinal host expression and microbiome analyses. Patients who met CDC VAP criteria with negative TA culture, patients who met clinical VAP criteria, and patients with pneumonia upon intubation were excluded. See Supplementary Data File 8 for more details. **B)** The Venn diagram on the left illustrates that patients were included at the "early" timepoint, the "late" timepoint, or both, depending on sample availability. The Venn diagram on the right shows that subjects were included in the bulk sequencing analysis, the single-cell analysis, or both, again dependent on sample availability. Abbreviations: VAP=ventilator-associated pneumonia; TA=tracheal aspirate; QC=quality control; PNA=pneumonia; CDC=United States Centers for Disease Control and Prevention.

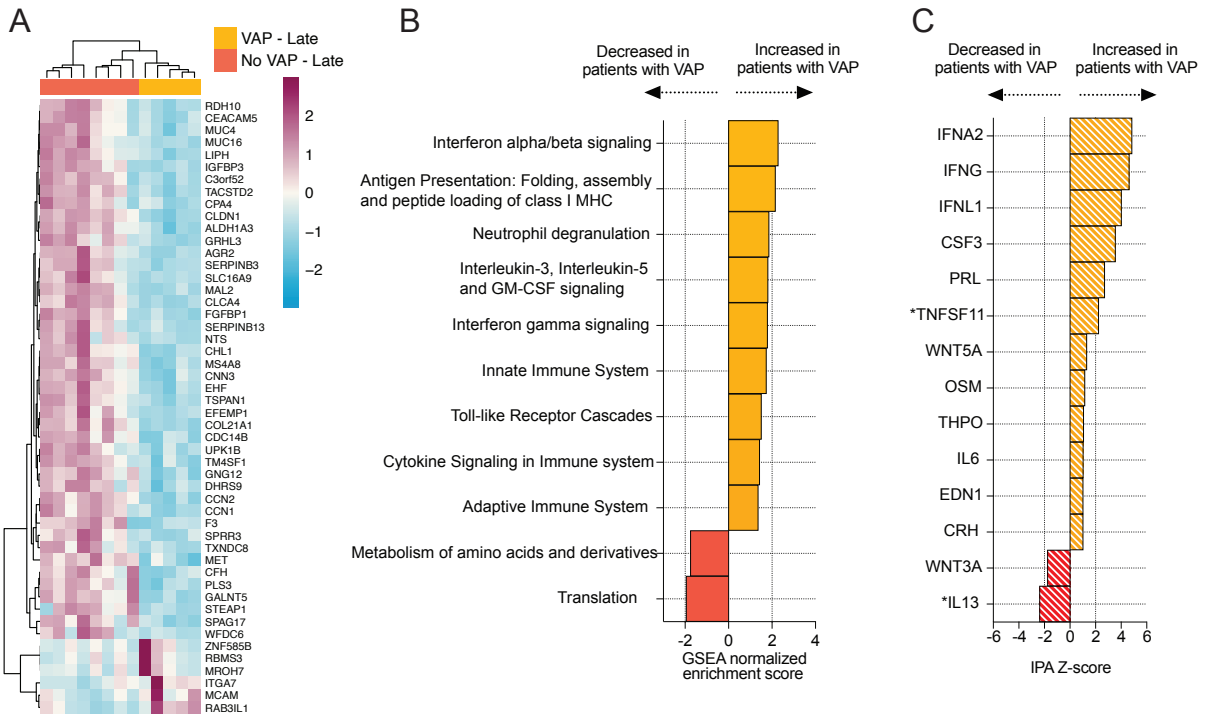

Figure 2: COVID-19 VAP is associated with a lower respiratory tract transcriptional signature of bacterial infection 2 days before VAP onset.
A) Heatmap of the top 50 differentially expressed genes by adjusted P-value between COVID-19 patients who developed VAP (yellow) versus those who did not (red) at the “late” timepoint, two days before the onset of VAP, from bulk RNA-seq. **B)** Gene set enrichment analysis (GSEA) at the “late” timepoint based on differential gene expression analyses. GSEA results were considered significant with an adjusted P-value < 0.05. **C)** Ingenuity Pathway Analysis (IPA) of upstream cytokines at the “late” timepoint based on differential gene expression analyses. IPA results were considered significant with a Z-score absolute value > 2 and overlap P-value < 0.05. *Denotes cytokines that were included with an overlap P-value < 0.1. All pathways and cytokines are shown in Supplementary Data Files 2 and 3.

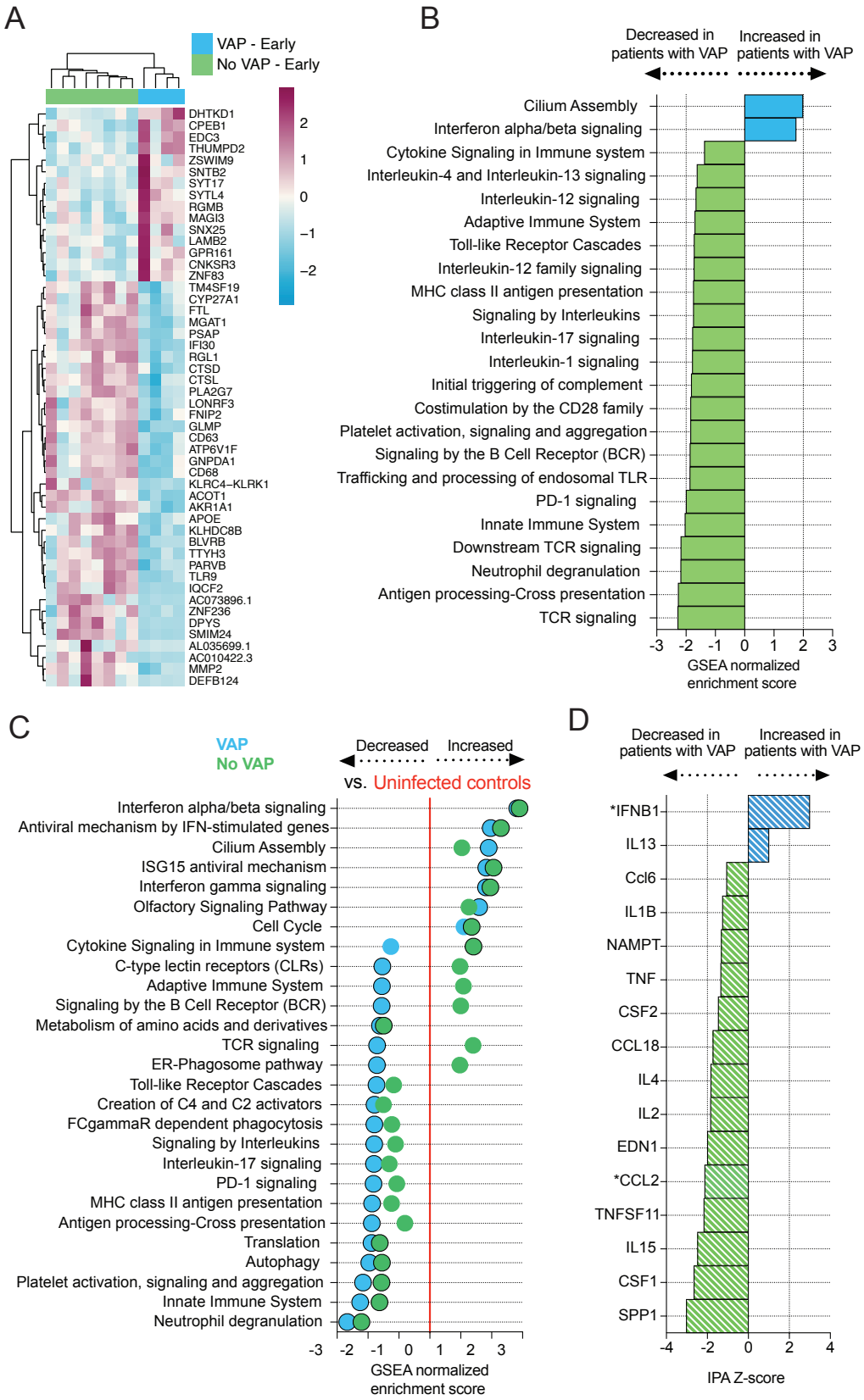
A
VAP - Early
No VAP - Early
DHTKD1
CPEB1
EDC3
THUMPD2
ZSWIM9
SNTB2
SYT17
SYTL4
RGMB
MAGI3
SNX25
LAMB2
GPR161
CNKSR3
ZNF83
TM4SF19
CYP27A1
FTL
MGAT1
PSAP
IFI30
RGL1
CTSD
CTSL
PLA2G7
LONRF3
FNIP2
GLMP
CD63
ATP6V1F
GNPDA1
CD68
KLRC4–KLRK1
ACOT1
AKR1A1
APOE
KLHDC8B
BLVRB
TTYH3
PARVB
TLR9
IQCF2
AC073896.1
ZNF236
DPYS
SMIM24
AL035699.1
AC010422.3
MMP2
DEFB124
2
1
0
−1
−2
B
Decreased in patients with VAP
Increased in patients with VAP
Cilium Assembly
Interferon alpha/beta signaling
Cytokine Signaling in Immune system
Interleukin-4 and Interleukin-13 signaling
Interleukin-12 signaling
Adaptive Immune System
Toll-like Receptor Cascades
Interleukin-12 family signaling
MHC class II antigen presentation
Signaling by Interleukins
Interleukin-17 signaling
Interleukin-1 signaling
Initial triggering of complement
Costimulation by the CD28 family
Platelet activation, signaling and aggregation
Signaling by the B Cell Receptor (BCR)
Trafficking and processing of endosomal TLR
PD-1 signaling
Innate Immune System
Downstream TCR signaling
Neutrophil degranulation
Antigen processing-Cross presentation
TCR signaling
-3 -2 -1 0 1 2 3
GSEA normalized enrichment score
C
VAP
No VAP
Decreased
Increased
vs. Uninfected controls
Interferon alpha/beta signaling
Antiviral mechanism by IFN-stimulated genes
Cilium Assembly
ISG15 antiviral mechanism
Interferon gamma signaling
Olfactory Signaling Pathway
Cell Cycle
Cytokine Signaling in Immune system
C-type lectin receptors (CLRs)
Adaptive Immune System
Signaling by the B Cell Receptor (BCR)
Metabolism of amino acids and derivatives
TCR signaling
ER-Phagosome pathway
Toll-like Receptor Cascades
Creation of C4 and C2 activators
FCgammaR dependent phagocytosis
Signaling by Interleukins
Interleukin-17 signaling
PD-1 signaling
MHC class II antigen presentation
Antigen processing-Cross presentation
Translation
Autophagy
Platelet activation, signaling and aggregation
Innate Immune System
Neutrophil degranulation
-3 -2 -1 0 1 2 3
GSEA normalized enrichment score
D
Decreased in patients with VAP
Increased in patients with VAP
*IFNB1
IL13
Ccl6
IL1B
NAMPT
TNF
CSF2
CCL18
IL4
IL2
EDN1
*CCL2
TNFSF11
IL15
CSF1
SPP1
-4 -2 0 2 4
IPA Z-score

755

Figure 3: COVID-19 patients who develop VAP have attenuated immune signaling in the lower respiratory tract two weeks before onset of secondary bacterial pneumonia.
A) Heatmap of the top 50 differentially expressed genes by adjusted P-value between COVID-19 patients who developed VAP (blue) versus those who did not (green) at the "early" timepoint from bulk RNA-seq. **B)** Gene set enrichment analysis at the "early" timepoint based on differential gene expression analyses. GSEA results were considered significant with an adjusted P-value < 0.05. **C)** Expression of GSEA pathways at the "early" timepoint with respect to a baseline of uninfected, intubated controls. Pathways were selected from the GSEA results if they had an adjusted P-value < 0.05 in at least one of the comparisons (VAP vs controls or No-VAP vs controls). Pathways with an adjusted P-value < 0.05 when compared to controls are indicated by circles with a black outline. **D)** Ingenuity Pathway Analysis (IPA) of upstream cytokine activation states at the "early" timepoint based on differential gene expression analyses. IPA results were considered significant with a Z-score absolute value > 2 and overlap P-value < 0.05. *Denotes cytokines that were included with an overlap P-value < 0.1. All pathways and cytokines are shown in Supplementary Data Files 2 and 3.

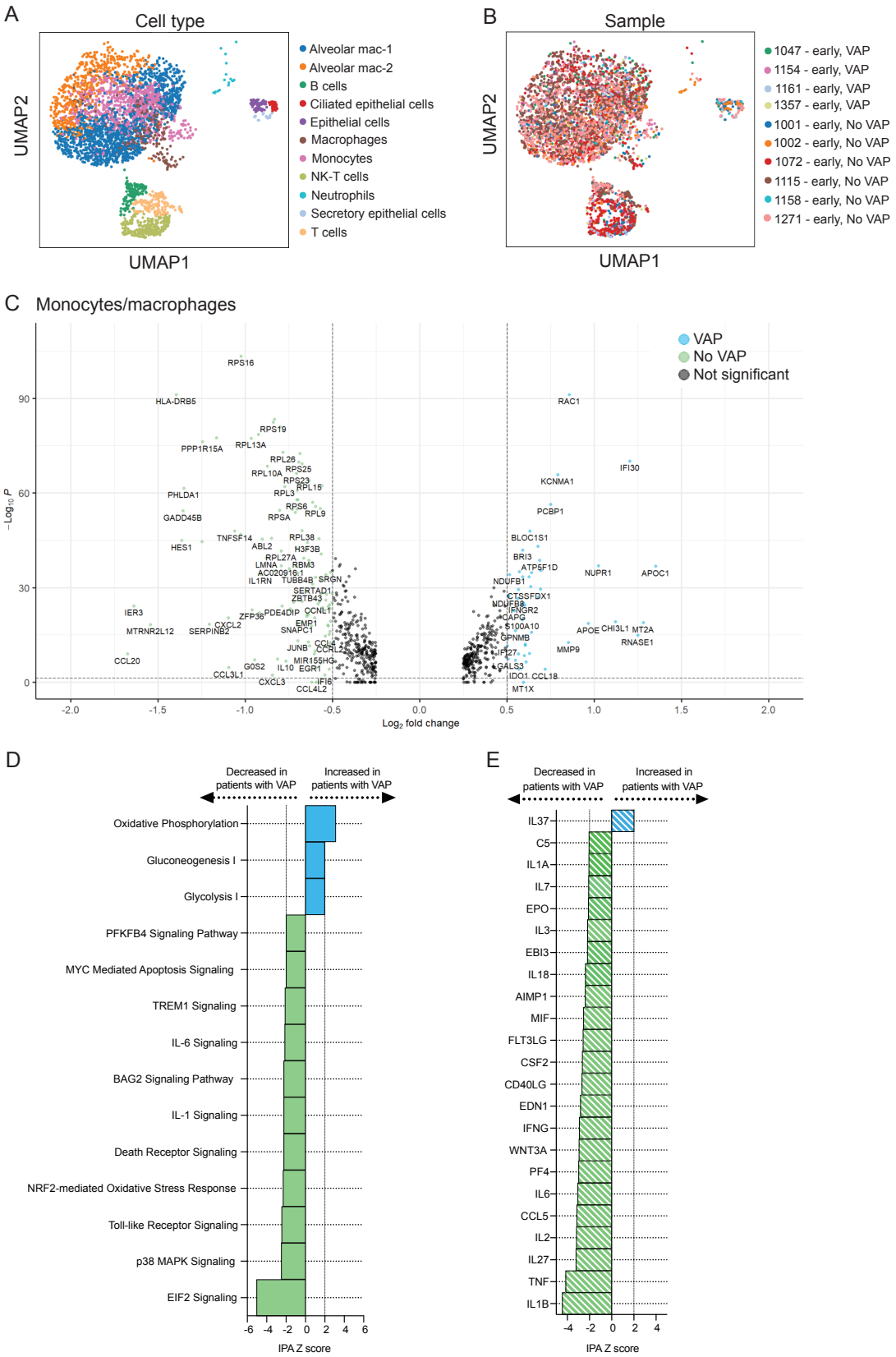
A
Cell type
UMAP2
UMAP1
Alveolar mac-1
Alveolar mac-2
B cells
Ciliated epithelial cells
Epithelial cells
Macrophages
Monocytes
NK-T cells
Neutrophils
Secretory epithelial cells
T cells
B
Sample
1047 - early, VAP
1154 - early, VAP
1161 - early, VAP
1357 - early, VAP
1001 - early, No VAP
1002 - early, No VAP
1072 - early, No VAP
1115 - early, No VAP
1158 - early, No VAP
1271 - early, No VAP
C Monocytes/macrophages
VAP
No VAP
Not significant
−Log10 P
Log2 fold change
D
Decreased in patients with VAP
Increased in patients with VAP
Oxidative Phosphorylation
Gluconeogenesis I
Glycolysis I
PFKFB4 Signaling Pathway
MYC Mediated Apoptosis Signaling
TREM1 Signaling
IL-6 Signaling
BAG2 Signaling Pathway
IL-1 Signaling
Death Receptor Signaling
NRF2-mediated Oxidative Stress Response
Toll-like Receptor Signaling
p38 MAPK Signaling
EIF2 Signaling
IPA Z score
E
Decreased in patients with VAP
Increased in patients with VAP
IL37
C5
IL1A
IL7
EPO
IL3
EBI3
IL18
AIMP1
MIF
FLT3LG
CSF2
CD40LG
EDN1
IFNG
WNT3A
PF4
IL6
CCL5
IL2
IL27
TNF
IL1B
IPA Z score

771

772 **Figure 4: scRNA-seq demonstrates that COVID-19 VAP is associated with early impaired**
773 **antibacterial immune signaling in lower respiratory tract monocytes and macrophages.**
774 **A-B)** UMAP of single cell RNA-seq data from patients that do or do not develop VAP at the "early"
775 timepoint, annotated by (A) cell type or (B) sample. **C)** Volcano plot displaying the differentially
776 expressed genes between VAP and No-VAP patients in the low-resolution
777 monocytes/macrophages cluster. **D-E)** Ingenuity Pathway Analysis (IPA) of (D) key canonical
778 pathways and (E) upstream cytokines based on differential gene expression analysis in
779 monocytes/macrophages of COVID-19 patients who developed VAP versus those who did not.
780 Only significant pathways (IPA Z-score absolute value > 2 and overlap P-value < 0.05) are
781 depicted. All pathways and cytokines are provided in Supplementary Data Files 5 and 6.

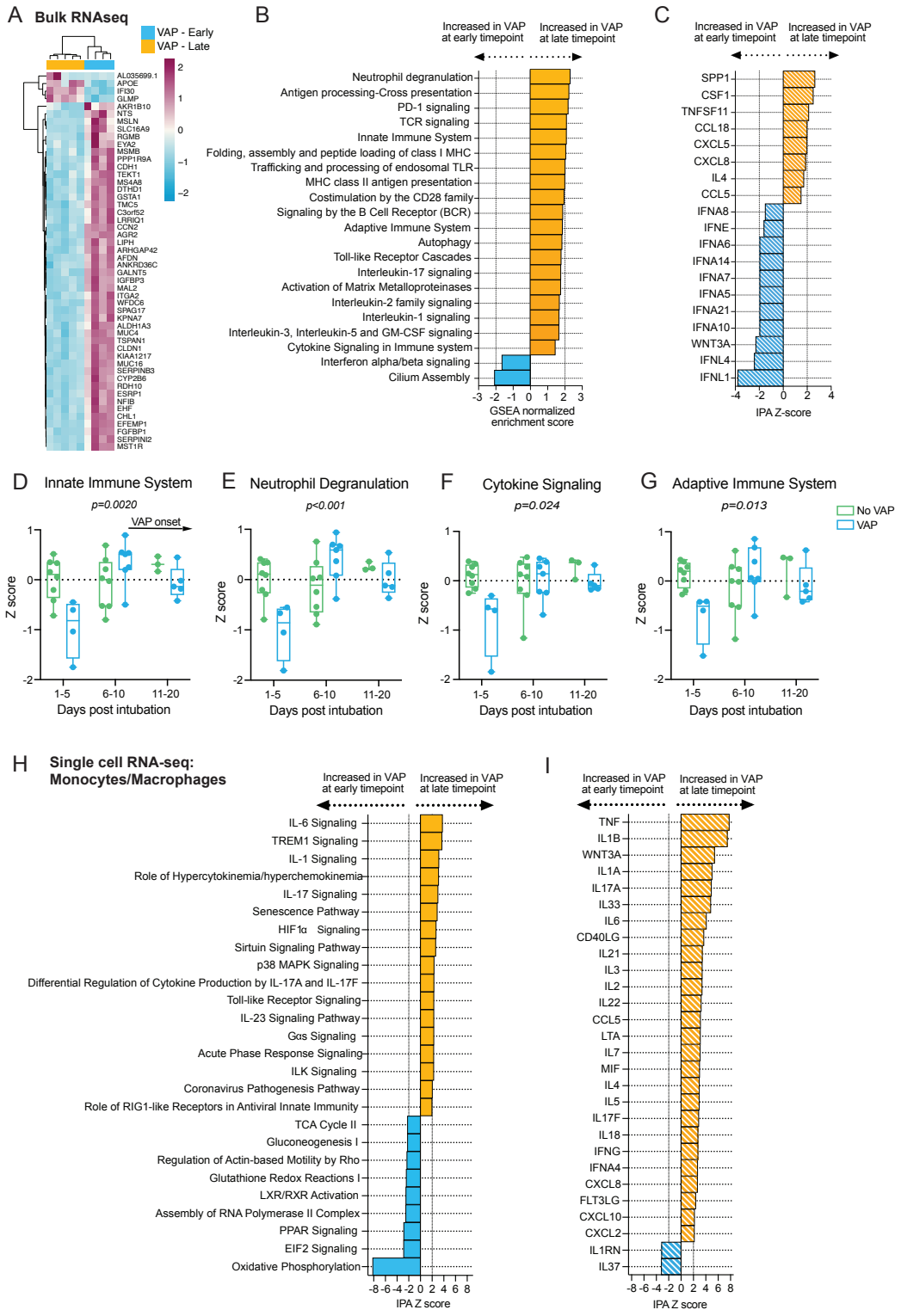
A Bulk RNAseq
VAP - Early
VAP - Late
B
Increased in VAP at early timepoint
Increased in VAP at late timepoint
Neutrophil degranulation
Antigen processing-Cross presentation
PD-1 signaling
TCR signaling
Innate Immune System
Folding, assembly and peptide loading of class I MHC
Trafficking and processing of endosomal TLR
MHC class II antigen presentation
Costimulation by the CD28 family
Signaling by the B Cell Receptor (BCR)
Adaptive Immune System
Autophagy
Toll-like Receptor Cascades
Interleukin-17 signaling
Activation of Matrix Metalloproteinases
Interleukin-2 family signaling
Interleukin-1 signaling
Interleukin-3, Interleukin-5 and GM-CSF signaling
Cytokine Signaling in Immune system
Interferon alpha/beta signaling
Cilium Assembly
GSEA normalized enrichment score
C
SPP1
CSF1
TNFSF11
CCL18
CXCL5
CXCL8
IL4
CCL5
IFNA8
IFNE
IFNA6
IFNA14
IFNA7
IFNA5
IFNA21
IFNA10
WNT3A
IFNL4
IFNL1
IPA Z-score
D Innate Immune System
p=0.0020
VAP onset
E Neutrophil Degranulation
p<0.001
F Cytokine Signaling
p=0.024
G Adaptive Immune System
p=0.013
No VAP
VAP
Z score
Days post intubation
1-5
6-10
11-20
H Single cell RNA-seq: Monocytes/Macrophages
IL-6 Signaling
TREM1 Signaling
IL-1 Signaling
Role of Hypercytokinemia/hyperchemokinemia
IL-17 Signaling
Senescence Pathway
HIF1α Signaling
Sirtuin Signaling Pathway
p38 MAPK Signaling
Differential Regulation of Cytokine Production by IL-17A and IL-17F
Toll-like Receptor Signaling
IL-23 Signaling Pathway
Gαs Signaling
Acute Phase Response Signaling
ILK Signaling
Coronavirus Pathogenesis Pathway
Role of RIG1-like Receptors in Antiviral Innate Immunity
TCA Cycle II
Gluconeogenesis I
Regulation of Actin-based Motility by Rho
Glutathione Redox Reactions I
LXR/RXR Activation
Assembly of RNA Polymerase II Complex
PPAR Signaling
EIF2 Signaling
Oxidative Phosphorylation
IPA Z score
I
TNF
IL1B
WNT3A
IL1A
IL17A
IL33
IL6
CD40LG
IL21
IL3
IL2
IL22
CCL5
LTA
IL7
MIF
IL4
IL5
IL17F
IL18
IFNG
IFNA4
CXCL8
FLT3LG
CXCL10
CXCL2
IL1RN
IL37

782

783 **Figure 5: Temporal dynamics of the host response to VAP**
784 **A)** Heatmap of the top 50 differentially expressed genes by adjusted P-value between COVID-19
785 patients who developed VAP at the "early" timepoint (blue) versus the "late" timepoint (yellow)
786 from bulk RNA-seq. **B)** Gene set enrichment analysis (GSEA) based on differential gene
787 expression of VAP patients at the "early" vs "late" timepoint from bulk RNA-seq. GSEA results
788 were considered significant with an adjusted P-value < 0.05. **C)** Ingenuity Pathway Analysis (IPA)
789 of upstream cytokine activation states based on differential gene expression analyses of VAP
790 patients at the "early" vs "late" timepoint from bulk RNA-seq. IPA results were considered
791 significant with a Z-score absolute value > 2 and overlap P-value < 0.05. **D-G)** Longitudinal
792 analysis of selected pathway expression in VAP (blue) versus No-VAP (green) patients from bulk
793 RNA-seq samples taken from time of intubation to onset of VAP for all patients. Pathway Z-scores
794 were calculated by averaging Z-scores for the top 20 leading edge genes of each pathway,
795 determined by the results of GSEA comparing VAP versus No-VAP patients at the "early"
796 timepoint. Multiple Z-scores per patient at a given time interval were averaged so that each patient
797 corresponds to one datapoint at each interval. Samples from day 21+ after intubation are not
798 depicted due to a lack of these later timepoints in the No-VAP group. VAP onset in these patients
799 ranged from 10-39 days post intubation (median: 19 days). Selected pathways are: innate
800 immune system (D), neutrophil degranulation (E), cytokine signaling (F), and adaptive immune
801 system (G). Box plots represent the median and range. Statistical significance was determined
802 by two-way ANOVA, and interaction P-values are highlighted. **H-I)** Ingenuity Pathway Analysis
803 (IPA) of (H) key canonical pathways (I) and upstream cytokine activation states based on
804 differential gene expression analysis in monocytes/macrophages from scRNA-seq of COVID-19
805 patients who developed VAP versus those who did not. Only significant pathways (IPA Z-score
806 absolute value > 2 and overlap P-value < 0.05) are depicted. All pathways and cytokines are
807 provided in Supplementary Data Files 2, 3, 5, and 6.

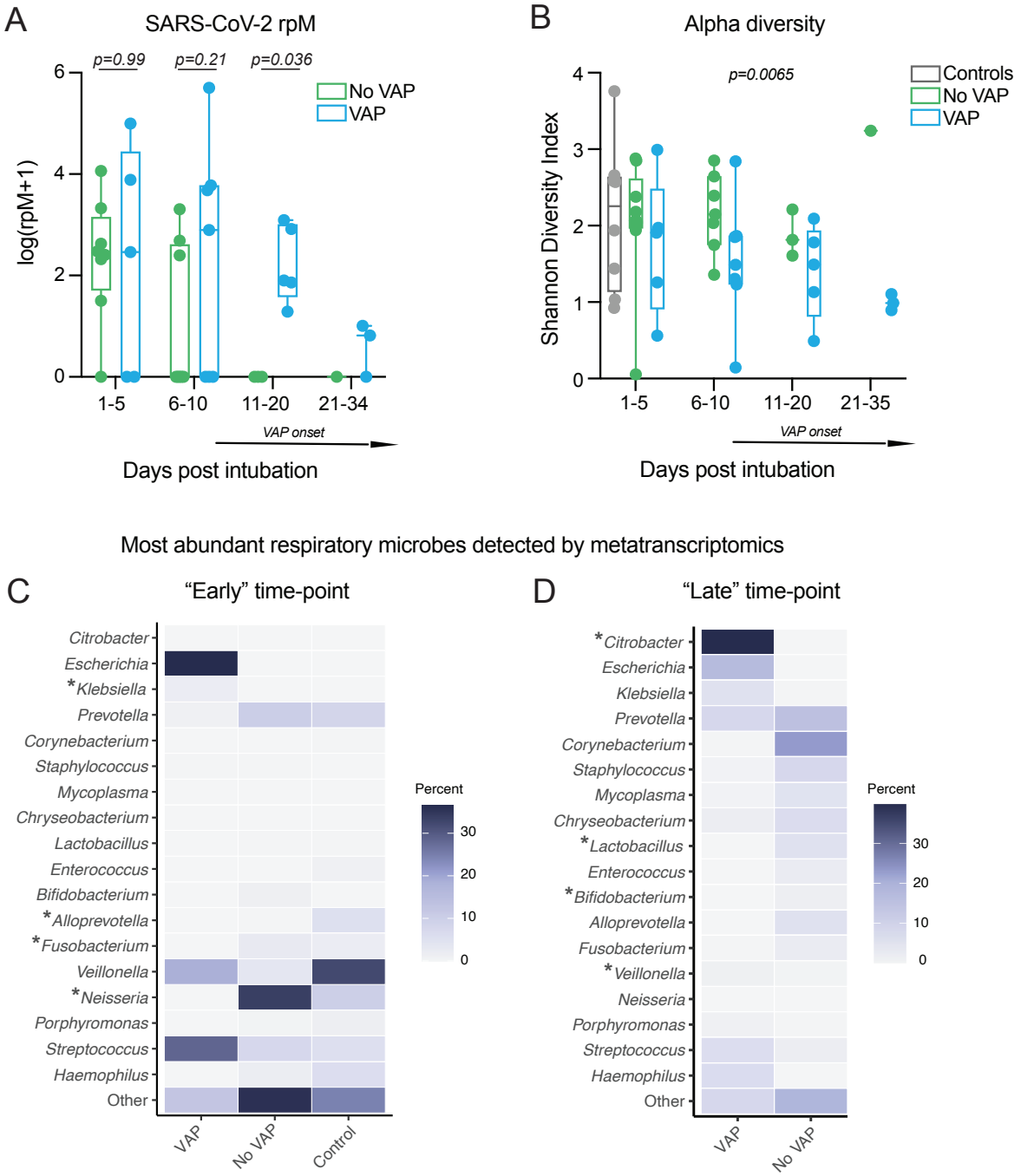

Figure 6: Lung microbiome community collapse precedes VAP in COVID-19 patients. **(A)** SARS-CoV-2 viral load (reads per million sequenced, rpM) over time by days since intubation in patients who develop VAP vs those who do not. For plotting purposes, log(rpM+1) was used to avoid negative values. **(B)** Lung microbiome bacterial diversity (Shannon's Index) in COVID-19 patients with relation to VAP development over time by days since intubation. VAP onset in these patients ranged from 10-39 days post intubation (median: 19 days). SARS-CoV-2 negative

816 intubated controls are included for comparison. Box plots represent the median and range.
817 Statistical significance was determined by Mann-Whitney tests (A) or two-way ANOVA between
818 VAP and No-VAP patients (B). P-values < 0.05 were considered significant. **(C-D)** Most abundant
819 respiratory microbes detected by metatranscriptomics at the (C) “early” and (D) “late” timepoints.
820 The mean abundance of the top 10 most abundant microbes from each group is depicted, and
821 significantly enriched taxa in VAP patients compared to No-VAP patients are marked by an
822 asterisk. SARS-CoV-2 negative intubated controls are included for comparison at the “early”
823 timepoint. Microbe abundance data for each patient can be found in Supplementary Data File 7.

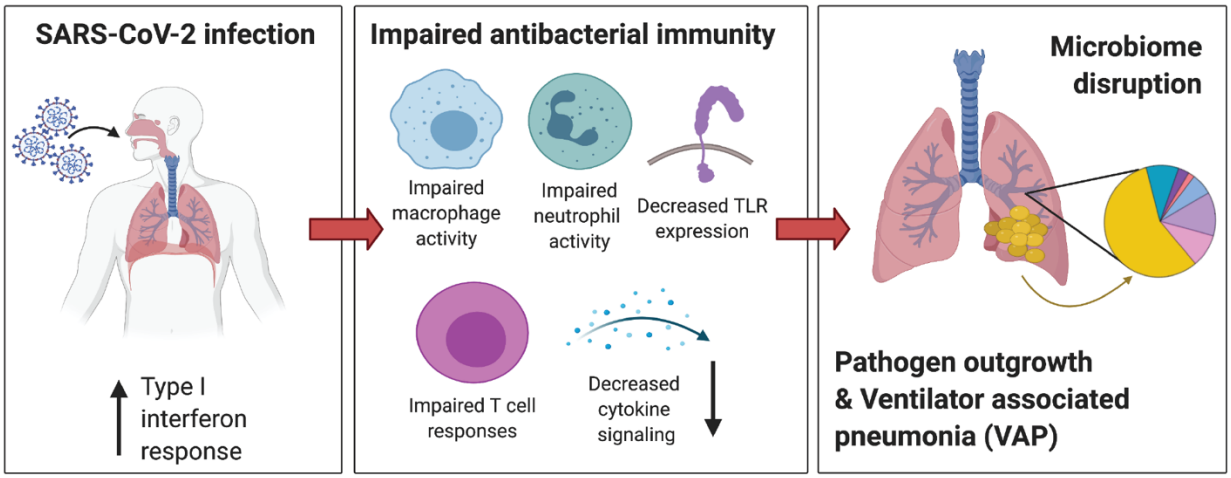

Figure 7: Mechanistic hypothesis of secondary bacterial pneumonia susceptibility in patients with COVID-19.
We hypothesize that individual immune responses to SARS-CoV-2 infection may drive a restructuring of the microbial community and increase susceptibility to VAP. Those predisposed to VAP have increased type I interferon responses and dysregulated antibacterial immune signaling characterized by impaired macrophage, neutrophil and T cell activity, decreased toll-like receptor (TLR) signaling and impaired activation of cytokines important for pathogen defense. This state of suppressed immunity may disrupt the lower respiratory tract microbiome, predisposing certain patients to the outgrowth of bacterial pathogens and VAP. Created with BioRender.com.